Since January 2020 Elsevier has created a COVID-19 resource centre with free information in English and Mandarin on the novel coronavirus COVID-19. The COVID-19 resource centre is hosted on Elsevier Connect, the company's public news and information website.

Elsevier hereby grants permission to make all its COVID-19-related research that is available on the COVID-19 resource centre - including this research content - immediately available in PubMed Central and other publicly funded repositories, such as the WHO COVID database with rights for unrestricted research re-use and analyses in any form or by any means with acknowledgement of the original source. These permissions are granted for free by Elsevier for as long as the COVID-19 resource centre remains active.

Biochimica et Biophysica Acta 1828 (2013) 1271–1283

Contents lists available at SciVerse ScienceDirect

Biochimica et Biophysica Acta

journal homepage: www.elsevier.com/locate/bbamem

Investigation of interfacial behavior of glycyrrhizin with a lipid raft model via a Langmuir monolayer study

Seiichi Sakamoto [a], Hiromichi Nakahara [a], Takuhiro Uto [b], Yukihiro Shoyama [b], Osamu Shibata [a,*]

[a] Department of Biophysical Chemistry, Faculty of Pharmaceutical Sciences, Nagasaki International University, 2825-7 Huis Ten Bosch, Sasebo, Nagasaki 859-3298, Japan
[b] Department of Pharmacognosy, Faculty of Pharmaceutical Sciences, Nagasaki International University, 2825-7 Huis Ten Bosch, Sasebo, Nagasaki 859-3298, Japan

ARTICLE INFO

Article history:
Received 31 July 2012
Received in revised form 8 January 2013
Accepted 9 January 2013
Available online 16 January 2013

Keywords:
Glycyrrhizin
Langmuir monolayer
Lipid raft
Membrane disruption
Saponin

ABSTRACT

An interaction of glycyrrhizin (GC) with a lipid raft biomembrane model that consisted of *N*-palmitoyl-D-*erythro*-sphingosylphosphorylcholine (PSM), 1,2-dioleoyl-*sn*-glycero-3-phosphocholine (DOPC), and cholesterol (CHOL) was systematically studied using the Langmuir monolayer technique. To construct the lipid raft model, the surface pressure (π)–molecular area (A) and surface potential (ΔV)–A isotherms for three-component (PSM/DOPC/CHOL) systems on 0.02 M Tris buffer with 0.13 M NaCl (pH 7.4) were primarily measured by changing their compositions. Thermodynamic and interaction parameters for binary PSM/DOPC and PSM/CHOL systems revealed that PSM interacts more strongly with CHOL than with DOPC. In addition, a morphological analysis performed with Brewster angle microscopy (BAM) and fluorescence microscopy (FM) revealed an optimal ratio of PSM/DOPC/CHOL (1/1/1, by mole) as a model of lipid rafts. Second, the interaction of GC with the ternary PSM/DOPC/CHOL monolayers was investigated on Tris buffer solutions containing different GC concentrations (1, 5, 10, 25, and 50 μM). In BAM and FM images, microdomains were found to become smaller by increasing the GC concentration in the subphase, suggesting that GC regulates the size of raft domains, which provide dynamic scaffolding for numerous cellular processes. More interestingly, the distinctive GC striped regions were formed at the interface at 50 μM, which shows that GC divides the ternary monolayer into pieces. This phenomenon was observed only in the presence of CHOL in the monolayer. These results suggest that CHOL plays an essential role in the interaction with GC, which results in one of the major activities associated with saponins' membrane disruption.

© 2013 Elsevier B.V. All rights reserved.

1. Introduction

Recently, the demand for Japanese traditional herbal medicines, the so-called Kampo medicines, has been dramatically increasing due to the rising concerns with health foods and complementary and alternative medicines [1]. The root of licorice belonging to the genus *Glycyrrhiza*, including *Glycyrrhiza uralensis* and *Glycyrrhiza glabra* (Chinese licorice), is the most widely used natural resource in Japanese traditional herbal medicines and is included in more than 70% of prescribed Kampo medicines. Furthermore, licorice has also been extensively utilized worldwide as a sweetener, tobacco flavoring agent, and food additive, and in cosmetics and confectionery foods [2]; accordingly, it has been recently named "Medicinal Plant of the Year 2012". A major bioactive compound of licorice, glycyrrhizin (GC; Fig. 1) has been shown to exhibit numerous pharmacological activities such as hepatoprotective [3], anti-inflammatory [4,5], anti-cariogenic [6], and anti-tumor activities [7]. In addition, various antiviral activities against coronavirus associated with severe acute respiratory syndrome [8], Newcastle disease virus, herpes simplex virus type 1, vesicular stomatitis virus [9], human immunodeficiency virus type 1 [10,11], influenza A virus [12], and hepatitis A virus [13] have been extensively studied. Due to these outstanding activities, GC has been clinically used for the treatment of allergies and chronic viral hepatitis for more than 50 years [14]. Moreover, GC has attracted much attention as a food additive, especially in "natural sweetener" with a low calorific value, because it has been shown to exhibit a sweetness 50-times more potent than that of sucrose [15]. Physicochemical properties of 18α- (trans-configuration at the C-18 position) and 18β-GC (cis-configuration at C-18 position) have been investigated by Kondo et al. [16]. These have been found to display interesting properties, particularly with respect to surface activity [17–19] and gel formation [20]. Because of the structural characteristics of amphiphiles, both exhibit interfacial activities with a critical micelle concentration (CMC) of ca. 0.2 mM, which was determined by measuring the interfacial tension at water–liquid paraffin interface at 25 °C. A notable dissimilarity between the physicochemical properties of the two isomers is related to their abilities to form gels. The aqueous solution of 18β-GC forms an extremely rigid gel even at a dilute concentration of less than 0.1 wt% (1.2 mM) at below pH 4.5, whereas 18α-GC does not.

Microdomains rich in sphingomyelin (SM) and cholesterol (CHOL), which are commonly referred to as lipid rafts, have been a subject of

* Corresponding author. Tel./fax: +81 956 20 5686.
E-mail address: wosamu@niu.ac.jp (O. Shibata).
URL: http://www.niu.ac.jp/~pharm1/lab/physchem/indexenglish.html (O. Shibata).

0005-2736/$ – see front matter © 2013 Elsevier B.V. All rights reserved.
http://dx.doi.org/10.1016/j.bbamem.2013.01.006

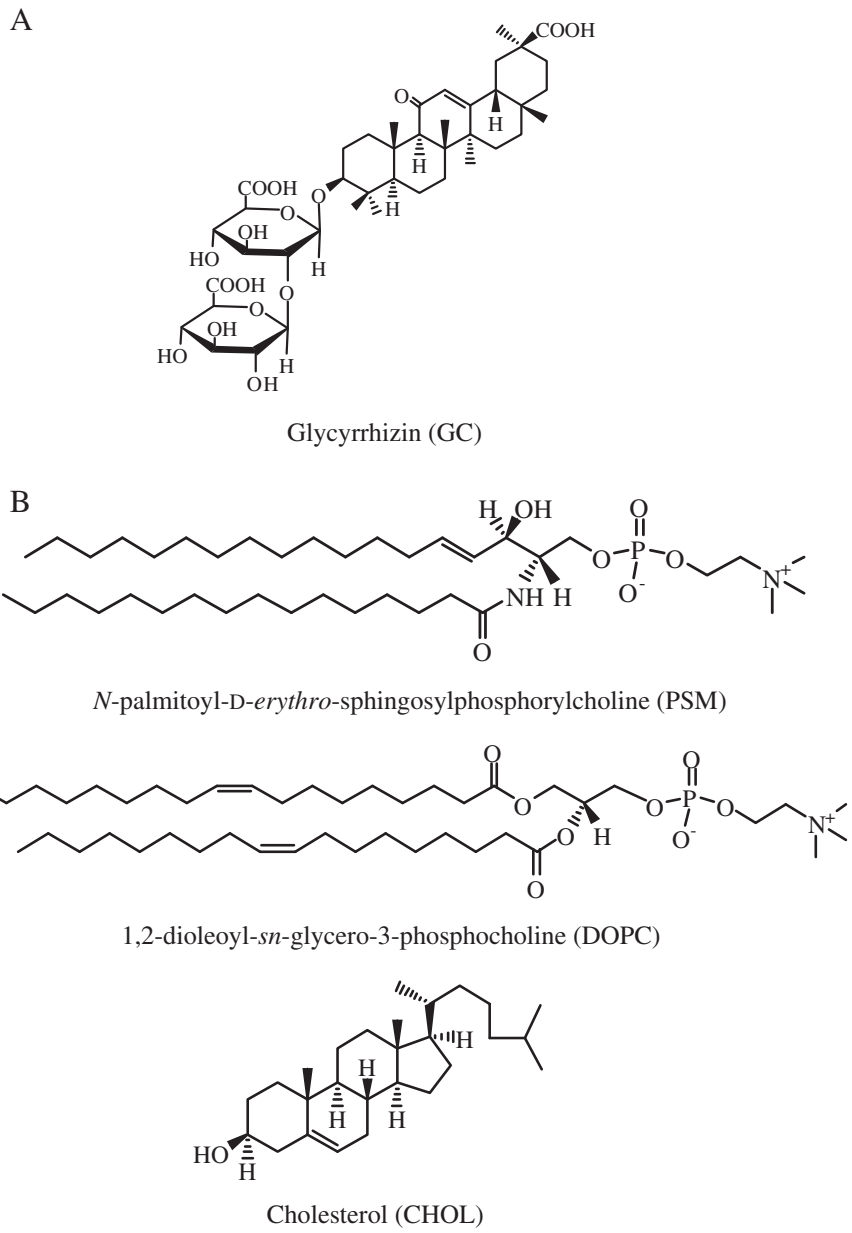

Fig. 1. Structures of (A) glycyrrhizin (GC) and (B) *N*-palmitoyl-D-*erythro*-sphingosylphosphorylcholine (PSM), 1,2-dioleoyl-*sn*-glycero-3-phosphocholine (DOPC), and cholesterol (CHOL).

great interest in cell biology because the significant membrane proteins involved in their physiological functions may be located selectively within them. Accordingly, they constantly provide dynamic scaffolding for various different cellular processes, including protein trafficking, signal transduction, and transportation of CHOL and membrane [21,22]. In rafts, long saturated acyl chains in sphingolipids (both SM and glycosphingolipids) are believed to tightly interact and to be packed with CHOL, which results in organization of liquid-ordered (l_o) phases [23–26]. By contrast, unsaturated phospholipids are loosely packed to form liquid-disordered (l_d) phases. These different packing properties lead to phase separation [27]. To elucidate liquid–liquid immiscibility in membranes, a large number of physicochemical studies on lipid rafts have been performed using a lipid mixture that mimics components of the outer leaflet of plasma membranes, in which the combination of sphingolipids, phospholipids, and CHOL has been most widely utilized. Recently, the monolayer technique, in combination with the Langmuir–Blodgett method [28], atomic force microscopy (AFM) [29–32], Brewster angle microscopy (BAM) [33,34], and various kinds of fluorescence microscopy (FM) [35–41], has been extensively performed using raft-mimicking lipid mixtures in order to examine their lateral organization. These methods enable a significant amount of important information concerning phase variations on micro- and nano-scales at the air/water interface to be obtained.

The behavior of GC on plasma membranes was evaluated by Nakamura et al. using cultured rat hepatocytes treated with hepatotoxin [42]. Release of glutamic-oxaloacetic transaminase and lactic dehydrogenase, which is induced by hepatotoxin, is significantly reduced by increasing the concentration of GC. These results suggest that GC directly prevents enzyme leakage by changing membrane permeability of hepatocytes. More recently, Harada reported the anti-viral strategy of GC and showed that the inhibition of viral infection by GC is mainly due to the suppression of fluidity of the plasma membrane and viral envelope into which GC is incorporated [43]. Interestingly, in both cases, GC acts to lower fluidity of the plasma membrane. However,

morphological changes related to the ability of GC to suppress membrane fluidity remain unknown.

GC is structurally classified as a triterpenoid saponin that possesses both hydrophobic (triterpenoid skeleton) and hydrophilic moieties (glucuronic acid) in the molecule. Saponins have been shown to cause membrane perturbation, which is frequently referred to as the hemolytic activity of saponins [44–48]. The molecular mechanism for the membrane-permeabilizing activity of saponins and steroidal glycoalkaloids has been proposed [49,50]. Briefly, saponins integrate with their hydrophobic part to form a complex with sterols, and formation of this complex promotes interaction of their extra-membranous orientated saccharide moieties, which results in their accumulation into plaque. Steric interference of these saccharide moieties causes membrane curvature, which subsequently leads to pore formation [49] or vesiculation [50] in the membrane. Alternatively, after their integration into the membrane, saponins may migrate toward sphingolipid/sterol-enriched membrane domains before forming a complex with the incorporated sterols, thereby interfering with specific domain functionalities [51]. However, morphological observation that strongly supports this hypothesis has not yet been reported.

Herein, we have investigated the effect of GC on a lipid raft model by employing the Langmuir monolayer technique. As representative components of lipid rafts in the model membrane, *N*-palmitoyl-D-*erythro*-sphingosylphosphorylcholine (PSM), 1,2-dioleoyl-*sn*-glycero-3-phosphocholine (DOPC), and CHOL (Fig. 1) were used. In the present study, we focused on the interaction of GC adsorbed from the subphase solutions with the raft model monolayer. The surface pressure (π)–molecular area (A) and surface potential (ΔV)–A for single, binary, and ternary monolayers composed of PSM, DOPC, and CHOL in the absence and the presence of GC in the subphase were primarily measured under physiological pH and ionic-strength conditions. Subsequently, GC dose-dependent phase behavior and domain variation of the model membrane were morphologically revealed using BAM and FM.

2. Materials and methods

2.1. Materials

N-palmitoyl-D-*erythro*-sphingosylphosphorylcholine (PSM; purity > 99%), 1,2-dioleoyl-*sn*-glycero-3-phosphocholine (DOPC; purity > 99%), and 1-palmitoyl-2-{6-[(7-nitro-2-1,3-benzoxadiazol-4-yl)amino] hexanoyl}-*sn*-glycero-3-phosphocholine (NBD-PC; purity > 99%) were purchased from Avanti Polar Lipids, Inc. (Alabaster, AL, USA). Cholesterol (CHOL; purity ≥ 99%) was obtained from Sigma Chemical. Co. (St. Louis, MO, USA). These lipids were used without further purification or characterization. Chloroform (99.7%) and methanol (99.8%), used as spreading solvents, were purchased from Kanto Chemical Co., Inc. (Tokyo, Japan) and nacalai tesque (Kyoto, Japan), respectively. Tris(hydroxymethyl) aminomethane (Tris), sodium chloride (NaCl), and acetic acid of guaranteed reagent grade for the preparation of a subphase were obtained from nacalai tesque (Kyoto, Japan). To exclude all surface-active organic impurities, NaCl was roasted at 1023 K for 24 h before use. The substrate solution was prepared using thrice distilled water (surface tension = 72.0 mN m^{-1} at 298.2 K; electrical resistivity = 18 MΩ cm).

2.2. Purification of glycyrrhizin (GC)

The compound 18β-GC (98%) obtained from nacalai tesque (Kyoto, Japan) required purification due to the presence of an impurity band in the thin-layer chromatography analysis. Further purification of GC was carried out by reverse-phase column chromatography using COSMOSIL (nacalai tesque, Kyoto, Japan). GC (5.0 g) was dissolved in 10 mL of 70% (v/v) methanol and applied to COSMOSIL gel (5.0 cm × 55.0 cm) equilibrated with 70% methanol. GC was then eluted with 3.0 L of the mobile phase (70% methanol) to give 4.5 g of purified GC. This purification was repeated seven times to obtain approximately 30 g of purified GC. The purity of GC was then measured by high-performance liquid chromatography analysis using two pumps (DP-8020, Tosoh Corp., Tokyo, Japan), connected with a UV detector (UV-8020, Tosoh Corp., Tokyo, Japan, 254 nm), degasser (SD-8022, Tosoh Corp., Tokyo, Japan), and an RP-18 column (TSK-GEL ODS-100 V, 250 mm × 4.6 mm, 5 μm, Tosoh Corp., Tokyo, Japan). The mobile phase consisted of 40% acetonitrile that contained 2% acetic acid was used at a flow rate of 0.7 mL min^{-1}. The purity of GC was estimated to be ≥98% according to the peak-area percentage method applied to the obtained chromatogram.

2.3. Surface pressure–area isotherms

The surface pressure (π) of monolayers was measured using an automated homemade Wilhelmy balance. The resolution of the surface pressure balance (Mettler Toledo, AG-245) was 0.01 mN m^{-1}. The pressure-measuring system was equipped with filter paper (Whatman 541, periphery = 4 cm). The trough was made from Teflon-coated brass (area = 750 cm^2), and both hydrophobic and lipophobic Teflon barriers were used in this study. Surface pressure (π)–molecular area (A) isotherms were recorded at 298.2 ± 0.1 K. Stock solutions of PSM (0.5 mM), DOPC (0.5 mM), and CHOL (1.0 mM) were prepared in chloroform/methanol (2/1, v/v). Spreading solvents were allowed to evaporate for 15 min before compression. The monolayer was compressed at a speed of ~0.10 nm^2 per molecule (without considering GC molecules) per minute. Standard deviations (SD) for the molecular surface area and surface pressure were ~0.01 nm^2 and ~0.1 mN m^{-1}, respectively. The pH of the subphase (0.02 M Tris buffer with 0.13 M NaCl) was adjusted to 7.4 with acetic acid.

2.4. Surface potential–area isotherms

The surface potential (ΔV) was recorded simultaneously with surface pressure when the monolayer was compressed at the air/water interface. This potential was monitored with an ionizing ^{241}Am electrode at 1–2 mm above the interface, whereas a reference electrode was dipped into the subphase. An electrometer (Keithley 614) was used to measure surface potential. SD of surface potential was 5 mV.

2.5. Surface tension measurements

The surface tension (γ) of surfactant solutions was determined at 298.2 K by using a drop volume tensiometer (YHC-2010, YTS, Japan) [52], which measures the volume of a drop detaching from a capillary with a known diameter. Temperature was maintained constant within ± 0.03 K by means of a thermostat. The experimental error in estimation of surface tension was ± 0.05 mN m^{-1}.

2.6. Brewster angle microscopy (BAM)

The monolayer was directly visualized by using a Brewster angle microscope (KSV Optrel BAM 300, KSV Instruments, Finland) coupled to a commercially available film balance system (KSV Minitrough, KSV Instruments, Finland). The use of a 20-mW He–Ne laser emitting *p*-polarized light with a wavelength of 632.8 nm and an instrument that was equipped with a 10× objective lens enabled a lateral resolution of ~2 μm. The angle of the incident beam to the air/water interface was fixed to the Brewster angle (53.1°) at 298.2 K. The reflected beam was recorded with a high-grade charge coupled device (CCD) camera (EHDkamPro02, EHD Imaging GmbH, Germany), and BAM images were digitally stored on a computer hard disk.

2.7. Fluorescence microscopy (FM)

The film balance system (KSV Minitrough, KSV Instruments, Finland) was mounted onto the stage of an Olympus BX51W1 microscope (Tokyo, Japan) equipped with a 100-W mercury lamp (USH-1030L), an objective lens (SLMPlan 50×, SLMPlanFI 20×, working distance = 15 mm), and a 3CCD camera control unit (IKTU51CU, Toshiba, Japan). The samples for FM were prepared by addition of 1 mol% of the phospholipid fluorescent probe, NBD-PC, individually to the stock solutions. The images observed at excitation and emission wavelengths of 460 and 534 nm, respectively, were directly recorded onto the hard disk via an online image processor (DVgate Plus, Sony, Tokyo, Japan) connected to the microscope. Image processing and analysis were conducted using the Adobe Photoshop Elements ver. 9.0 (Adobe System Incorporated, CA, USA) software package. The total amount of ordered domains (dark contrast regions) was evaluated and expressed as a percentage per frame by dividing the respective frames into dark and bright regions.

2.8. Fabrication of GC layers adsorbed from the subphase

The Tris buffer solutions (0.02 M) with 0.13 M NaCl (pH 7.4) containing proper amounts of GC (1, 5, 10, 25, or 50 μM) were prepared as subphases. After clearing trough and barriers with chloroform and acetone, the subphase was poured into the trough. We then waited until an equilibrium state of GC adsorption from the subphase to surface was achieved. The equilibrium time of adsorption depended on the GC concentration in the subphase. After equilibrium, samples such as PSM, DOPC, CHOL, and their mixtures were spread onto the surface. The isotherm measurements and microscopic observations were made in the same manner as that previously described. Note that this is not the method where highly concentrated GC solutions are injected into the subphase. Solubility of GC in the aqueous solution is considerably low. Therefore, if we applied the injection method, large amounts of GC solutions would need to be injected so that the water level of the subphase would increase substantially. However, in the method used in the present study, there are errors in base values of π and ΔV; indeed, the isotherm data were obtained under the base of respective GC-containing Tris buffer not just Tris buffer. First, γ and ΔV values at an equilibrium state of GC in the 0.02 M Tris buffer solution with 0.13 M NaCl (pH 7.4) were measured to normalize the data obtained in this manner (see Fig. S1 in Supplementary material). Using these values, all $\pi - A$ and $\Delta V - A$ isotherms shown herein were normalized in subsequent procedures.

In the present study, experimental π ($=\pi_{exp}$) is obtained by Eq. (1):

$$\pi_{exp} = \gamma_{GC} - \gamma_m \tag{1}$$

where γ_{GC} denotes the surface tension of the GC-containing buffer solution at a certain concentration of GC (C_{GC}) and γ_m represents the surface tension of the monolayer on the GC-subphase. The γ_{GC} values were independently measured using the drop volume method (Fig. S1(A)). Herein, we define π_{GC} as follows:

$$\pi_{GC} = \gamma_0 - \gamma_{GC} \tag{2}$$

where γ_0 is the surface tension of the buffer solution without any surfactants. From Eqs. (1) and (2), π is offset so that the base value of π comes to become γ_0:

$$\pi = \pi_{exp} + \pi_{GC} = \gamma_0 - \gamma_m \tag{3}$$

The ΔV value can be normalized similarly. The experimental value (ΔV_{exp}) is expressed in Eq. (4):

$$\Delta V_{exp} = V_m - V_{GC} \tag{4}$$

where V_m and V_{GC} denote potentials of the subphase covered with the monolayer and those of the GC-containing buffer solution at a certain C_{GC}, respectively. In advance, surface potential (ΔV_{GC}) of GC solutions was obtained in the absence of lipid monolayers (Fig. S1(B)). The ΔV_{GC} value satisfies Eq. (5):

$$\Delta V_{GC} = V_{GC} - V_0 \tag{5}$$

where V_0 represents the potential of the buffer solution in the absence of surfactants. We can obtain the normalized value from Eqs. (4) and (5) as follows:

$$\Delta V = \Delta V_{exp} + \Delta V_{GC} = V_m - V_0 \tag{6}$$

That is, a zero of vertical axes of π and ΔV, plotted in the whole figures, means those of a non-covered surface of 0.02 M Tris buffer solution with 0.13 M NaCl (pH 7.4) in the absence of lipid monolayers and GC.

3. Results and discussion

3.1. One-component monolayers for N-palmitoyl-D-erythro-sphingosylphosphorylcholine (PSM), 1,2-dioleoyl-sn-glycero-3-phosphocholine (DOPC), and cholesterol (CHOL)

The surface pressure (π)–molecular area (A) and surface potential (ΔV)–A isotherms of representative PSM, DOPC, and CHOL were measured on 0.02 M Tris buffer with 0.13 M NaCl (pH 7.4) at 298.2 K (Fig. 2). The π–A isotherm of PSM shows a phase transition pressure (π^{eq}) of ~21 mN m^{-1} (solid arrow), at which the monolayer phase starts changing from a liquid-expanded (LE) to liquid-condensed (LC). The extrapolated area, which is the molecular area of the ordered-state part on the π–A isotherm at $\pi = 0$, of PSM is ~0.48 nm^2. DOPC forms a typical expanded monolayer with an extrapolated area of ~0.79 nm^2. In contrast, CHOL forms a typical condensed monolayer (liquid or solid state, see Fig. S2 in Supplementary material) with a limiting molecular area of ~0.38 nm^2, which is in good agreement with the cross-sectional area of CHOL molecules computed on the basis of average tilt angle [53]. Values of π^{eq}, phase collapse pressure (π^c), and its corresponding collapse area (A^c) of PSM, DOPC, and CHOL are shown in Table 1.

The surface potential (ΔV) generally reflects orientational and conformational changes of monolayers upon compression. The ΔV values of all monolayers vary positively upon compression, which means that the molecular orientation in a monolayer is improved in the direction normal to the surface plane [54]. When the PSM, DOPC, and CHOL monolayers are compressed up to the close-packed state, their ΔV values reach ~354, ~418, and ~401 mV, respectively. These results are in good agreement with those of previous studies [55–57]. In case of PSM, the slope of ΔV–A isotherm changes at ~0.51 nm^2 (indicated by an arrow), which corresponds to the LE/LC phase transition. This result suggests that molecular orientation of PSM is abruptly improved when the phase is changed from the LE to LC state.

In situ morphological observations for a one-component monolayer at the air/water interface were carried out by BAM and FM. BAM images of DOPC and CHOL monolayers show a homogeneous LE phase (dark contrast) and an LC phase (bright contrast), respectively (see Fig. S3(B), (C) in Supplementary material). As for PSM, the phase transition (π^{eq} = ~21 mN m^{-1}) from the LE to LC phase is observed when transition is judged from the dark–bright contrast (Fig. S3(A) in Supplementary material). In order to further investigate interfacial behaviors of one-component monolayers, FM possessing greater resolution and magnification was then performed, even though the doping probe was in the sample. Fig. 3 shows fluorescence images of PSM monolayers on 0.02 M Tris buffer (0.13 M NaCl, pH 7.4) at 298.2 K.

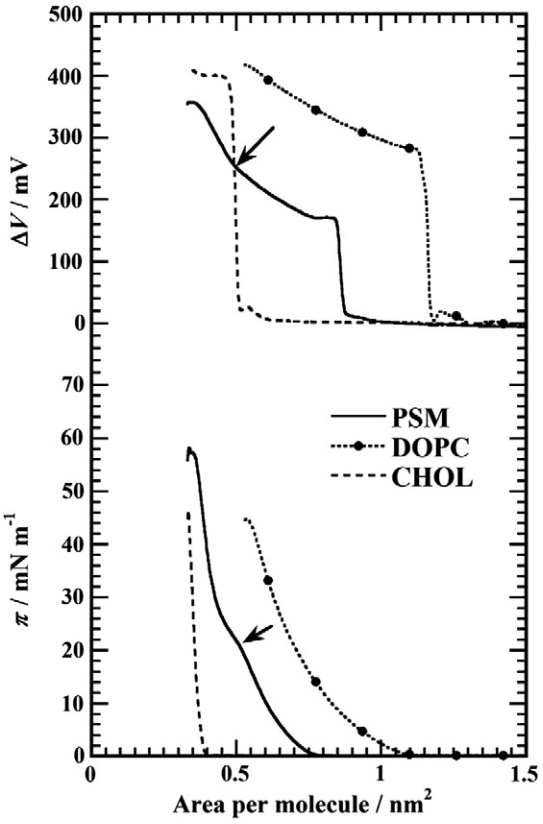

Fig. 2. The π–A and ΔV–A isotherms of pure PSM, DOPC, and CHOL monolayers spread on 0.02 M Tris buffer containing 0.13 M NaCl at 298.2 K (pH 7.4). Solid arrows in the isotherms indicate an LE/LC phase transition.

Fluorescent probes (here, NBD-PC) dissolve selectively into the LE phase in the monolayer state. Therefore, in contrary to bright and dark regions in BAM images, those in FM images correspond to LE and LC phases, respectively. Below $\pi^{eq} = \sim 21$ mN m^{-1}, FM images are homogeneously bright. However, the nucleation of LC domains is apparent at the transition point, and further compression leads to growth of LC domains in starburst-like shapes up to 25 mN m^{-1}. Above 30 mN m^{-1}, edges of LC domains become unclear. The size of LC domains in PSM remains constant, even though LC domains of 1,2-dipalmitoyl-*sn*-glycero-3-phosphocholine (DPPC) grow by lateral compression [58]. It is considerable that the degree of hydration around the head group of PSM, which possesses amine and hydroxyl groups, is stronger than that of DPPC, which reflects growth of LC domains by lateral compression.

3.2. Binary monolayers (PSM/DOPC and PSM/CHOL)

The π–A and ΔV–A isotherms of two-component (PSM/DOPC and PSM/CHOL) systems were measured on 0.02 M Tris buffer with 0.13 M NaCl (pH 7.4) at 298.2 K (Fig. 4). The isotherms of π–A and ΔV–A for PSM/DOPC system are shown in Fig. 4(A). The inset in Fig. 4(A) shows the mean area per molecule (A) of monolayers as a function of X_{PSM} at 25 mN m^{-1}. The dashed line was drawn assuming linear additivity, and solid points represent experimental values. The positive deviation from linearity suggests that PSM repulses DOPC by possessing double saturated chain that is considered to prevent packing of DOPC monolayers. In addition, the inset of Fig. 4(A) indicates that the π–A isotherms shift to smaller areas with increasing the molar fraction of PSM (X_{PSM}). As to π^{eq} variation, it decreases slightly within a range of ~5.0 mN m^{-1} as X_{PSM} increases ($0.8 \le X_{PSM} \le 1$), as evident in Figs. S4 and 6(A), whereas π^c values gradually vary between the monolayers of DOPC (*curve* 1) and PSM (*curve* 9) with increasing X_{PSM} ($0.7 \le X_{PSM} \le 1$) (Fig. 6(A)). With respect to ΔV values in this system, no obviously different behavior is observed, except that the ΔV values gradually decrease as X_{PSM} increases.

In the binary PSM/CHOL system (Fig. 4(B)), π–A isotherms overlap at $0 \le X_{PSM} \le 0.5$. In contrast to the binary PSM/DOPC system, the additivity of A as a function of X_{PSM} at 25 mN m^{-1} shows negative deviation, which implies that PSM attracts CHOL by possessing a large cavity to wrap the CHOL molecule. In addition, an almost constant mean area per molecule is observed over the range of $0 \le X_{PSM} \le 0.5$, which results from the overlap observed in the π–A isotherms (*curves* 1–4 in Fig. 4(B)). Further addition of PSM ($X_{PSM} \ge 0.7$) expands the isotherm to close to pure PSM monolayers (*curve* 8) which indicates the LE/LC phase transition at ~21 mN m^{-1} (solid arrow) at 298.2 K. The values of π^{eq} slightly decrease as X_{PSM} increases ($0.95 \le X_{PSM} \le 1$), whereas those of π^c gradually increase and reach a plateau at $X_{PSM} = 0.9$ (Fig. 6(B)). In ΔV–A isotherms, ΔV values increase and reach maxima at $X_{PSM} = 0.5$ and 0.7 ($\Delta V = \sim 437$ mV); then, they decrease to be almost the same as that of the isotherm of pure PSM (*curve* 8), where the ΔV value is ~354 mV. These results suggest that the PSM/CHOL monolayer is mostly packed at $0.5 \le X_{PSM} \le 0.7$.

The interaction parameter of PSM with DOPC or CHOL can be evaluated in terms of the excess Gibbs free energy of mixing, ΔG^{exc}. The ΔG^{exc} value is evaluated by integration of π–A isotherms from zero to a selected surface pressure on the basis of Eq. (7) [59]:

$$\Delta G^{exc} = \int_0^{\pi} (A_{12} - X_1 A_1 - X_2 A_2) d\pi \quad (7)$$

where A_i and X_i are the area per molecule and molar fraction of the component i, respectively, and A_{12} is the mean area per molecule in mixture of components 1 and 2. In absence of interactions between the two-components, $\Delta G^{exc} = 0$ [60,61]. The negative and positive deviations from ideality indicate intermolecular attraction and repulsion, respectively. Variations of ΔG^{exc} for the two-component PSM/DOPC and PSM/CHOL monolayers as function of X_{PSM} at five surface pressures are shown in Fig. 5. ΔG^{exc}–X_{PSM} curves in the PSM/DOPC system at five surface pressures are shown in Fig. 5(A). The ΔG^{exc} values are mostly positive and attain a maximum value at 40 mN m^{-1} at $X_{PSM} = 0.6$ (800 J mol^{-1}). Because their values increase with increasing surface pressure, repulsive interaction between PSM and DOPC is induced upon compression. In the PSM/CHOL system (Fig. 5(B)), contrary to the PSM/DOPC system, the ΔG^{exc} values are negative over the whole range of surface pressures. These results indicate that the interactions between PSM and CHOL are more attractive than PSM–PSM and CHOL–CHOL interactions. Obviously, these values decrease with increasing surface pressures. In particular, they reach ~−2500 J mol^{-1} at $0.5 \le X_{PSM} \le 0.7$ at 45 mN m^{-1}, which indicates that interaction between acyl chains of PSM and the skeleton of CHOL molecules becomes more attractive as intermolecular distance becomes shorter upon compression. In addition, the ranges ($0.5 \le X_{PSM} \le 0.7$) of the largest ΔG^{exc} values are agreed well with those of the largest ΔV values obtained from ΔV–A isotherms of PSM/CHOL (Fig. 4(B)). These results reflect the fact that lipid rafts organize liquid-ordered (l_o) phases by tightly packing between sphingolipids and CHOL [23–26]. That is, tight packing between PSM and CHOL improves the molecular orientation in the

Table 1
The phase transition pressure (π^{eq}), phase collapse pressure (π^c), and its corresponding collapse area (A^c) of PSM, DOPC, and CHOL.

	π^{eq} (mN m^{-1})	π^c (mN m^{-1})	A^c (nm^2)
PSM	21	57	0.36
DOPC		45	0.54
CHOL		47	0.34

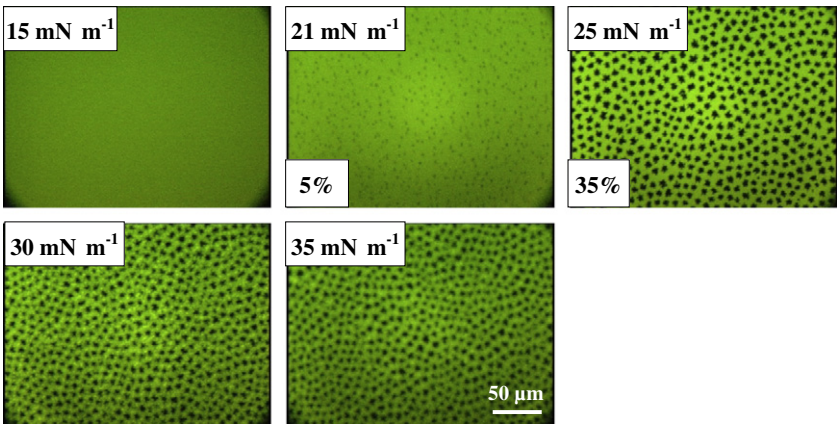

Fig. 3. FM micrographs of pure PSM monolayers on 0.02 M Tris buffer containing 0.13 M NaCl (pH 7.4) at 298.2 K. The monolayers contain 1 mol% of the fluorescent probe (NBD-PC). The scale bar at the lower-right represents 50 μm. The percentage (%) at the lower-left indicates the ratio of occupied LC domains against the frame.

PSM/CHOL system at $0.5 \leq X_{PSM} \leq 0.7$. These results also demonstrate that during monolayer compression, PSM attracts CHOL and repels DOPC. Notably, unsaturated aliphatic chains of DOPC monolayers are packed upon compression with π − π bonding. Thus, addition of PSM possessing double-saturated chains is considered to prevent monolayer packing of DOPC.

The interaction between DOPC and CHOL was investigated by the isotherm measurements (*π*–*A* and Δ*V*–*A* isotherms) and thermodynamic studies (ΔG^{exc} values) as a function of X_{CHOL} (Fig. S5). These results suggest that the strongest interaction exists at $X_{CHOL} = 0.5$ with minimum ΔG^{exc} values of -2000 J mol^{-1} at 40 mN m^{-1}, which are in good agreement with those in the previous study, indicating that DOPC and CHOL attractively interact each other, especially at $X_{CHOL} = 0.5$ [62]. However, a comparison between ΔG^{exc} values in the DOPC/CHOL system (-1800 J mol^{-1} at 35 mN m^{-1}) and those in the PSM/CHOL system (-2300 J mol^{-1} at 35 mN m^{-1}) suggests that CHOL interacts more strongly with PSM than with DOPC through hydrogen bonding. These results support the evidence that the amide nitrogen of sphingomyelin (SM) has a possibility to bind to the 3-OH group of CHOL [63,64] for their attractive interaction.

Studies of the two-dimensional phase diagram on the transition (π^{eq}) and the collapse (π^{c}) pressures in the Langmuir monolayer are

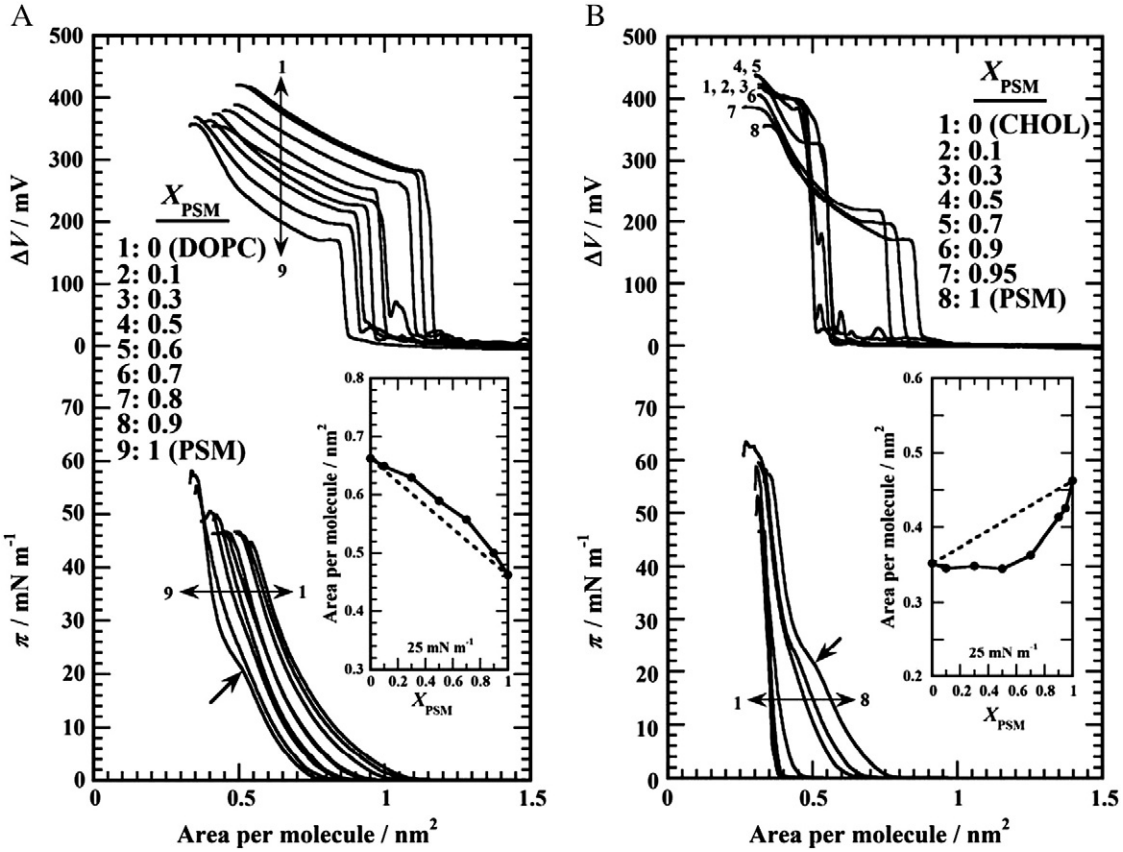

Fig. 4. The *π*–*A* and Δ*V*–*A* isotherms of the binary (A) PSM/DOPC and (B) PSM/CHOL monolayers on 0.02 M Tris buffer containing 0.13 M NaCl (pH 7.4) at 298.2 K. An inset indicates mean molecular area (*A*) of the monolayers as a function of X_{PSM} at 25 mN m^{-1}. Solid arrows represent an LE/LC phase transition at ~21 mN m^{-1}.

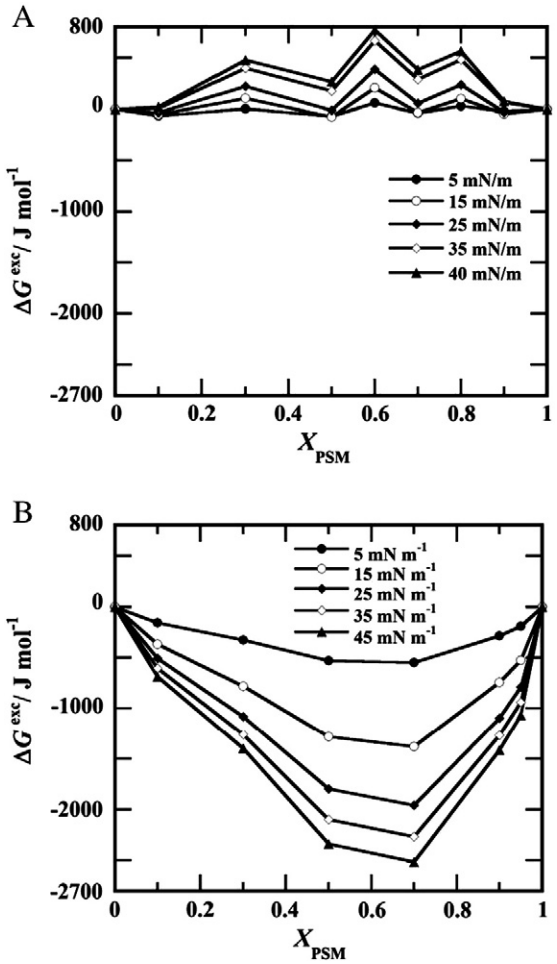

Fig. 5. Excess Gibbs free energy of mixing for the (A) PSM/DOPC and (B) PSM/CHOL monolayers as a function of X_{PSM} at five different surface pressures. ΔG^{exc} value was calculated from Eq. (7).

of much interest since they provide thermodynamic information related to phase behavior. Two-dimensional phase diagrams for binary systems were constructed by plotting π^{eq} and π^{c} values against X_{PSM} at 298.2 K (Fig. 6). For PSM/DOPC (Fig. 6(A)) and PSM/CHOL (Fig. 6(B)) systems, the π^{eq} change negatively as X_{PSM} increases at $0.8 \le X_{PSM} \le 1$ (see Fig. S4) and $0.95 \le X_{PSM} \le 1$, respectively. Regarding the PSM/DOPC system (Fig. 6(A)), the constant π^{c} ($0 \le X_{PSM} \le 0.7$) demonstrates that the two-components are immiscible at $0 \le X_{PSM} \le 0.7$ although the homogeneous domain (bright regions) is optically observed in FM and BAM images (Fig. S4). A nanometric technique such as AFM may be useful to morphologically investigate miscibility at $0 \le X_{PSM} \le 0.7$ in greater detail [65,66]. In the present study, however, immiscibility in the range of $0 \le X_{PSM} \le 0.7$ is clearly described on the basis of thermodynamic considerations. The two-component system is considered to be partially miscible because the PSM/DOPC system is miscible at $0.8 \le X_{PSM} \le 1$. On the other hand, considering the continuous change of π^{c} at $0 \le X_{PSM} \le 0.9$ and that of π^{eq} at $0.95 \le X_{PSM} \le 1$, the binary PSM/CHOL system is miscible in the monolayer state.

Assuming that binary monolayers behave as a regular surface mixture with a hexagonal lattice, the coexistence phase boundary between ordered monolayer (2-D phase) and bulk phases (3-D phase) of molecules spread on the surface can be theoretically simulated by the Joos equation [67]:

$$1 = x_1^s \exp\{(\pi_m^c - \pi_1^c)\omega_1/kT\} \exp\left\{\xi (x_2^s)^2\right\} + x_2^s \exp\{(\pi_m^c - \pi_2^c)\omega_2/kT\} \exp\left\{\xi (x_1^s)^2\right\} \quad (8)$$

where x_1^s and x_2^s denote the molar fractions in the two-component monolayers of components 1 and 2, respectively; π_1^c and π_2^c are the collapse pressures of components 1 and 2, respectively; π_m^c is the collapse pressure of the two-component monolayer at a given composition of x_1^s (or x_2^s); ω_1 and ω_2 are the corresponding areas per molecule at the collapse points; ξ is the interaction parameter; and kT is the product of the Boltzmann constant and absolute temperature. The solid curve at higher surface pressures was obtained by adjusting the interaction parameter in Eq. (8) to obtain the best fit for the experimental π^{c} values. As shown in Fig. 6, PSM/DOPC ($0.7 \le X_{PSM} \le 1$) and PSM/CHOL ($0 \le X_{PSM} \le 1$) systems show that $\xi = -0.40$ and $\xi = -0.59$, respectively. The negative interaction parameters imply higher interaction energy between the molecules relative to the mean energy of interaction between the same molecules.

Interaction energy ($\Delta\varepsilon$) is given as follows:

$$-\Delta\varepsilon = \xi RT/z \quad (9)$$

where z is the number of nearest neighbors (equal to 6) in a hexagonal close-packed, and the interaction energy is also described as $-\Delta\varepsilon = \varepsilon_{12} - (\varepsilon_{11} + \varepsilon_{22})/2$ [67]; ε_{ij} represents the potential energy of interaction between components i and j. The interaction energies were calculated to be 165 J mol^{-1} ($\xi = -0.40$) for PSM/DOPC system at $0.7 \le X_{PSM} \le 1$ and 244 J mol^{-1} ($\xi = -0.59$) for PSM/CHOL system. Because the interaction energies are less than $2RT$ (4958.7 J mol^{-1}), these two-components are miscible within the range described above.

3.3. Ternary monolayers (PSM/DOPC/CHOL)

The π–A and ΔV–A isotherms of three-component PSM/DOPC/CHOL systems are shown in Fig. 7. Since the sphingomyelin (SM) and phosphatidylcholine (PC) have been reported to be contained equally in the lipid raft fraction [68], the ratio of PSM/DOPC was fixed in this study. As shown in the figure, the ternary monolayers were investigated as functions of the amount of CHOL, where an equimolar ratio of PSM/DOPC (1/1, mol/mol) was maintained. The π–A isotherms appear to shift to small areas and show characteristics of condensed monolayers as the molar fraction of CHOL increases. In addition, π^{c} values slightly change by the addition of CHOL. Regarding ΔV–A isotherms, maximum ΔV values at the close-packed state increase from ~380 (*curve* 1) to ~460 mV (*curve* 6). These results indicate that the addition of CHOL improves monolayer packing of PSM rather than that of DOPC.

FM images of the ternary monolayers are shown in Figs. S6 and 8, in which corresponding BAM images are also inserted in the upper-right corner. For the PSM/DOPC (1/1) system without CHOL, both BAM and FM images are optically homogeneous over the whole range of surface pressures, even though microdomains of binary egg SM/DOPC (1/1) monolayers have been identified using AFM [31]. Microdomains (so-called raft domains) are observed after addition of a small amount of CHOL ($X_{CHOL} = 0.11$), and further addition of CHOL promotes their formation. Indeed, the percentage at the lower-left in the frame, which represents the ratio of occupied LC domains in the micrograph, increases as the CHOL amount increases ($0.11 \le X_{CHOL} \le 0.5$). At 25 mN m^{-1} (Figs. S6 and 8), the ratio of 84% at $X_{CHOL} = 0.5$ is greater than 50%. Considering characteristics of PSM (LE/LC) (Fig. 2) and DOPC (LE), LC domains are suggested to be composed of CHOL and PSM. This suggestion is also supported by the ΔG^{exc} analysis, which shows that PSM attractively interacts with CHOL and repulsively with DOPC, as shown in Fig. 5. Therefore, the raft domain of the PSM/DOPC/CHOL (1/1/1) monolayer is found to be CHOL-rich. Recent studies using PSM/DOPC/CHOL (1/1/1) with the same composition as that used in the present study have reported the round domains, which were assigned to a PSM/CHOL-rich l_o phase [32]. FM images also show that the percentages increase upon lateral

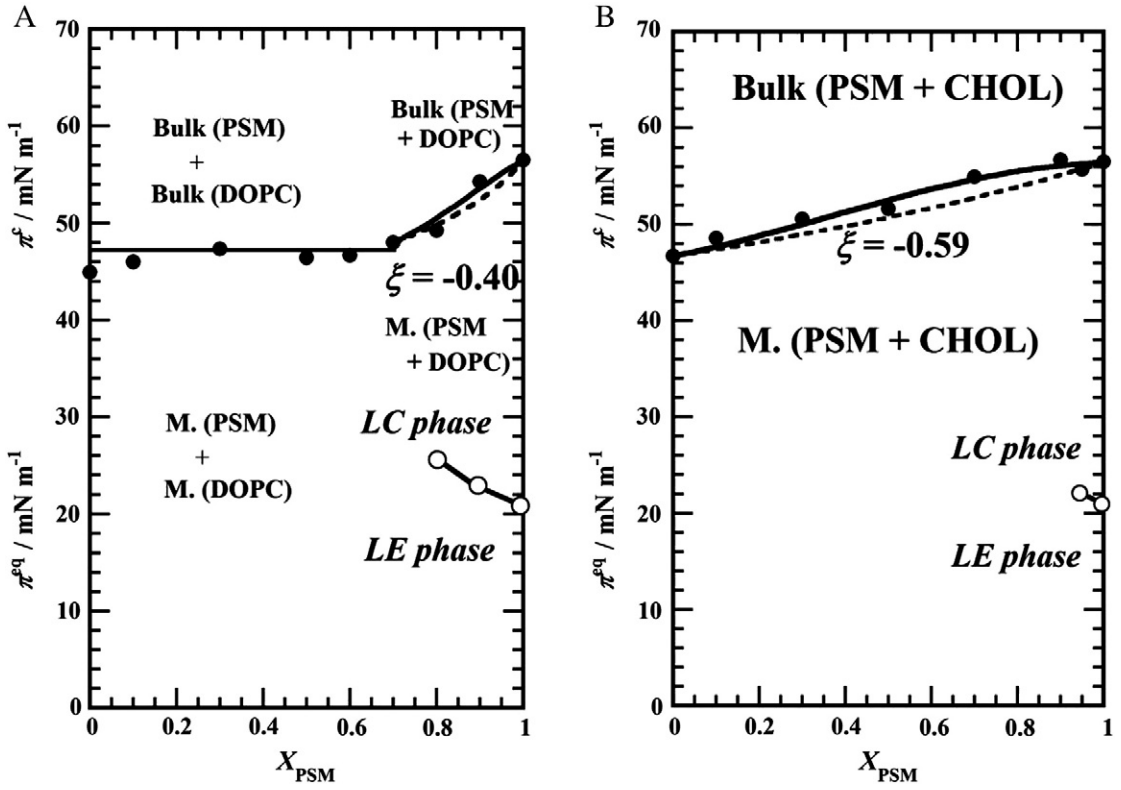

Fig. 6. Two-dimensional phase diagrams based on the variation of the transition pressure (π^{eq}: open circle) and collapse pressure (π^{c}: solid circle) as a function of X_{PSM}; (A) PSM/DOPC and (B) PSM/CHOL. The dashed lines were calculated according to Eq. (8). M. indicates a monolayer state. Bulk indicates a solid phase.

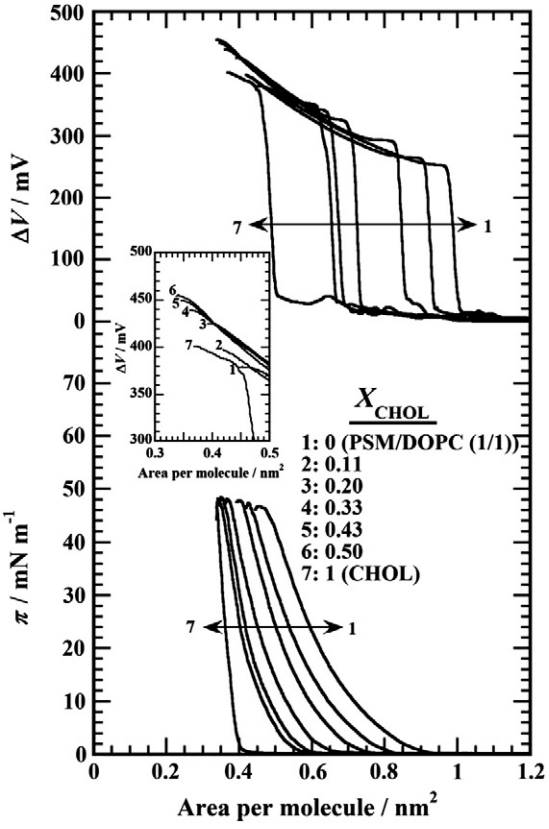

Fig. 7. The π–A and ΔV–A isotherms of the binary PSM/DOPC (=1/1, mol/mol) monolayer containing different amounts of CHOL on 0.02 M Tris buffer with 0.13 M NaCl (pH 7.4) at 298.2 K. (Inset) enlarged ΔV–A isotherms in the surface potential region of $300 \leq \Delta V$ (in mV) ≤ 500.

compression (Figs. S6 and 8). However, individual raft domains at $X_{CHOL} = 0.43$ and 0.50 are found to fuse to form larger submicron-sized domains below 35 mN m^{-1}, which corresponds to a lateral surface pressure of biomembrane [69–71]. These fusions are also reproduced in BAM images. On the other hand, at $X_{CHOL} = 0.33$, the fusion of LC raft domains does not occur until 35 mN m^{-1}. Therefore, the additional ratio of CHOL is 33% ($X_{CHOL} = 0.33$) in the equimolar binary PSM/DOPC monolayers, and the mixture of PSM/DOPC/CHOL (1/1/1) was selected as a model of lipid rafts in this study.

These results support the previously reported data regarding the effect of CHOL on the size or number of binary egg SM/DOPC (1/1) complexes (10–100 nm) [31]. According to the previous report, the size and number of domains are unaffected by the addition of CHOL to egg SM/DOPC (1/1) bilayers in concentrations up to ~15%. When the concentration of CHOL is 25%, however, the domains become much larger (1 μm in diameter). At 50% CHOL concentration in egg SM/DOPC bilayers, domains are on the order of 10 μm. In addition, the ternary phase diagram, using egg SM/PC/CHOL, allows us to postulate why high concentrations of CHOL induce this phenomenon. Egg SM/PC (1/1) mixtures are in the transition region between liquid-disordered (l_o) and solid-ordered phases (s_o). Therefore, the increase in the amount of CHOL leads to a modification of the domain topology (i.e., formation of l_o domains), which causes a large domain (i.e., disappearance of phase separation) at high molar fractions of CHOL [72].

3.4. Interaction of PSM/DOPC/CHOL (1/1/1) monolayer with GC

To elucidate the interaction of GC adsorbed from the subphase with the lipid raft model, which is the equimolar ternary PSM/DOPC/CHOL monolayer, π–A and ΔV–A measurements were performed. Fig. 9 shows π–A and ΔV–A isotherms of ternary monolayers on 0.02 M Tris buffer with 0.13 M NaCl (pH 7.4) containing different amounts of GC. The lower inserted π–time (t) isotherms represent dependence of the

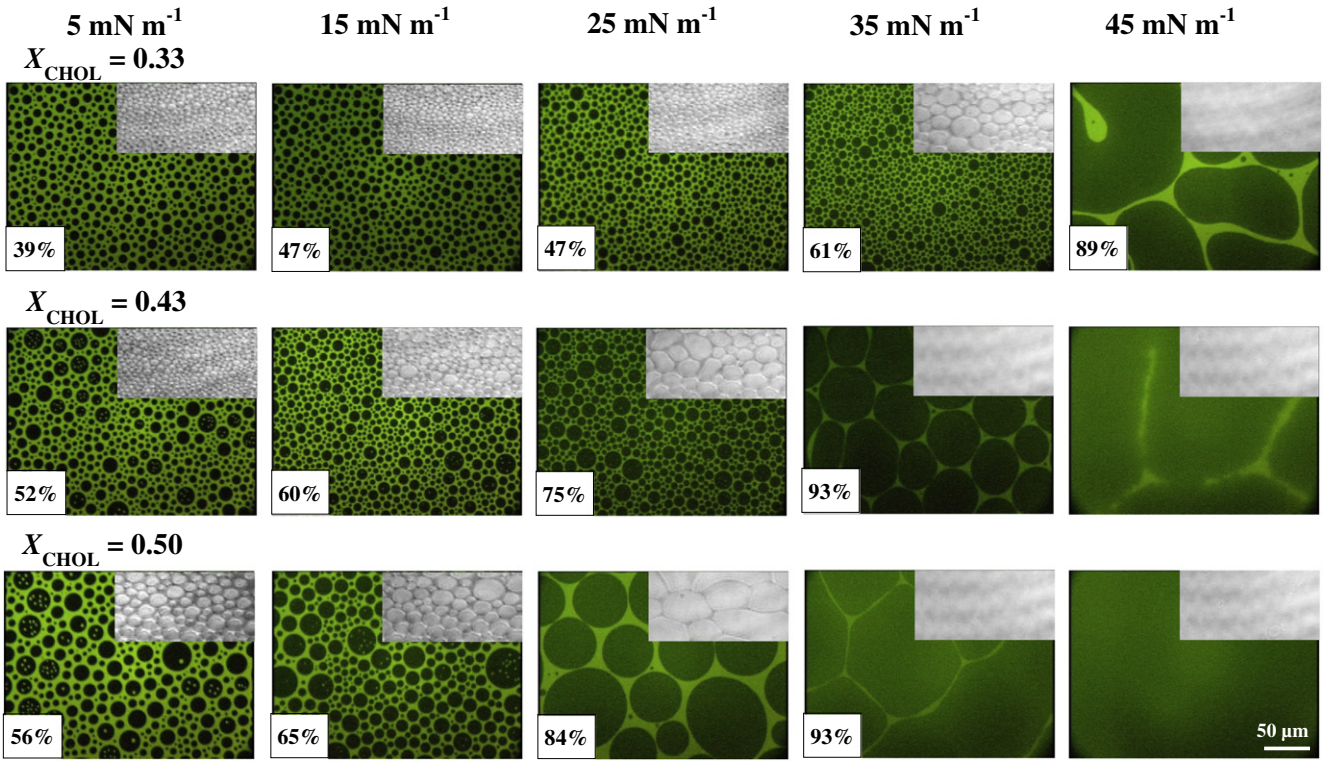

Fig. 8. Fluorescence micrographs of the binary PSM/DOPC (1/1, mol/mol) monolayer containing different amounts of CHOL at five surface pressures (5, 15, 25, 35, and 45 mN m^{-1}) on 0.02 M Tris buffer with 0.13 M NaCl (pH 7.4) at 298.2 K (X_{CHOL} = 0.33, 0.43 and 0.50). The monolayers contain 1 mol% of the fluorescent probe (NBD-PC). The scale bar in the lower-right represents 50 μm. The corresponding BAM images are shown in the upper-right of each photograph. The percentages represent the ratio of LC domains occupied in the frame.

adsorption time of GC from the bulk subphase to surface at different GC concentrations (C_{GC} = 1, 5, 10, 25, and 50 μM). These results indicate that GC attains adsorption equilibrium within 90 min at the previously noted GC concentrations. Therefore, PSM/DOPC/CHOL (1/1/1) monolayers were spread onto the GC solution at 90 min after the subphase containing GC was poured into the trough. The π–A isotherms of the PSM/DOPC/CHOL (1/1/1) monolayer are considerably expanded by increasing C_{GC}. However, it is estimated that these expansions attain saturation at C_{GC} = 100 μM since the π–A isotherm, obtained from C_{GC} = 100 μM, is overlapped with that obtained from C_{GC} = 50 μM (data not shown). In the close-packed state, all isotherms have almost the same π^c values of ~48 mN m^{-1} (A = ~0.36 nm^2). The effect of micelles of GC on PSM/DOPC/CHOL (1/1/1) monolayers was investigated by measuring π–A and ΔV–A isotherms at C_{GC} levels greater than or equal to critical micelle concentration (CMC) (see Fig. S7 in Supplementary material) [16]. The ΔV–A isotherms show that ΔV values on GC subphases finally converge to that without GC upon compression although initial ΔV values are relatively different depending on C_{GC}. As observed in the inserted upper figure, the maximum ΔV value at C_{GC} = 10 μM is greater by ~35 mV than that at C_{GC} = 0. A plausible explanation is that some GC molecules remain at the surface even in the close-packed state or almost all GC molecules are eliminated from the surface to be located just below the surface monolayer.

To verify the previous hypothesis, the isotherm measurements and morphological observations for single and binary monolayers were typically done at C_{GC} = 50 μM. As seen in Fig. 10, all π–A isotherms are expanded to larger areas compared with isotherms without GC (Figs. 2 and 4). At the closed-packed state, the molecular area above 40 mN m^{-1} for monolayers are similar to those for C_{GC} = 0, which means that most GC molecules are squeezed out of surface upon compression. It is noted that the positive slopes of ΔV–A isotherms of PSM at C_{GC} = 50 μM suddenly become negative slopes at a molecular area of ~0.81 nm^2 (π = ~19 mN m^{-1}), as indicated by a solid arrow. This dramatic negative change is possibly due to desorption of GC from the air/water interface, which occurred simultaneously with conformational changes of monolayers. It is supposed that the growth of LC domains of PSM excludes GC molecules from the interface because pure PSM has LE/LC phase transition at ~21 mN m^{-1} (Fig. 2). In addition, conditions under which formation of a subphase is possible (5 M NaCl) to stabilize GC monolayers (typical LE phases) due to the salting out effect are evident in Fig. S8. On the contrary, GC cannot form stable monolayers on the subphase with lower NaCl concentrations. Therefore, in the current system, GC molecules are considered to be desorbed from the air/water interface by compression. At a minimum point of convex upward for ΔV, where the molecular area is ~0.66 nm^2 at 24 mN m^{-1}, the slope again changes positively. This change means that the GC molecules are dramatically desorbed between surface pressures of ~19 and ~24 mN m^{-1}, which correspond to the molecular areas at start (~0.81 nm^2) and end (~0.66 nm^2) points of the negative slope upon compression. The GC monolayer has positive ΔV values of ~503 mV at the close-packed state (Fig. S8), and the adsorbed GC layer also indicates positive ΔV values (Fig. S1(B)). Thus, the reduction in ΔV value (negative slope) means that GC is desorbed into the bulk by compression so that the ΔV value of the desorbed GC is canceled because of electrostatic neutrality in the bulk. Similarly, the desorption timing of GC by other monolayers is also estimated by slope variations in ΔV–A isotherms as positive slopes change to negative slopes during desorption of GC. ΔV–A isotherms of DOPC-containing monolayers (DOPC and PSM/DOPC (1/1)) show that the slope changes negatively (dashed arrows). That is, GC is desorbed into the bulk between ~17 and ~19 mN m^{-1} for DOPC and between ~12 and ~15 mN m^{-1} for PSM/DOPC (1/1). On the contrary, as for ΔV–A isotherms of CHOL-containing monolayers (CHOL and PSM/CHOL (1/1)), GC is found to be desorbed between ~10 and 19 mN m^{-1} for CHOL and between ~16 and 20 mN m^{-1} for PSM/CHOL (1/1). However, the $\Delta V-A$ isotherms indicate no negative variations although the slopes change at surface pressures where GC begins to desorb from the surface, as opposed to other systems. Judging from

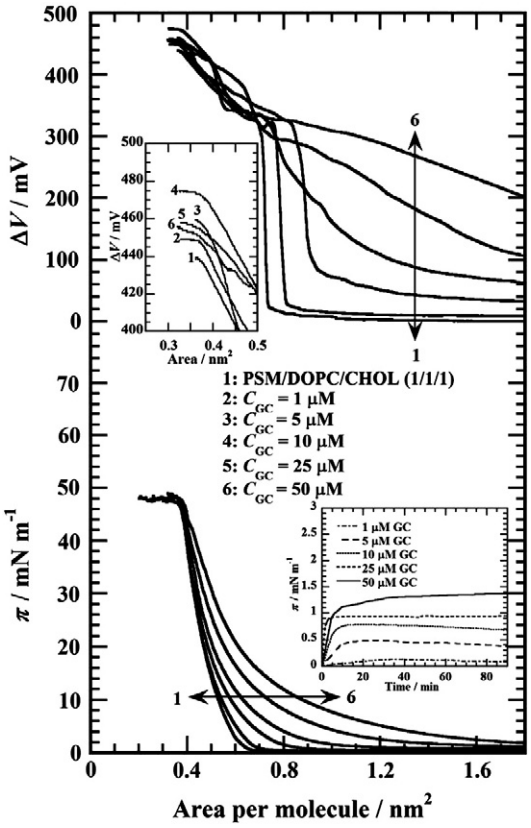

Fig. 9. The π–A and ΔV–A isotherms of the ternary PSM/DOPC/CHOL (1/1/1, by mol) monolayers on 0.02 M Tris buffer containing 0.13 M NaCl (pH 7.4) in the presence of different amounts of GC (C_{GC} = 1, 5, 10, 25, and 50 μM) at 298.2 K. The inset at the upper-left represents enlarged ΔV–A isotherms in the surface potential region of $400 \leq \Delta V$ (in mV) ≤ 500, while the inset at the lower-right exhibits π–t isotherms for adsorption of GC from the subphases containing different C_{GC}. Note that the area axis means mean molecular area of the PSM/DOPC/CHOL mixtures, where molecular weight and amount of adsorbed GC are not considered.

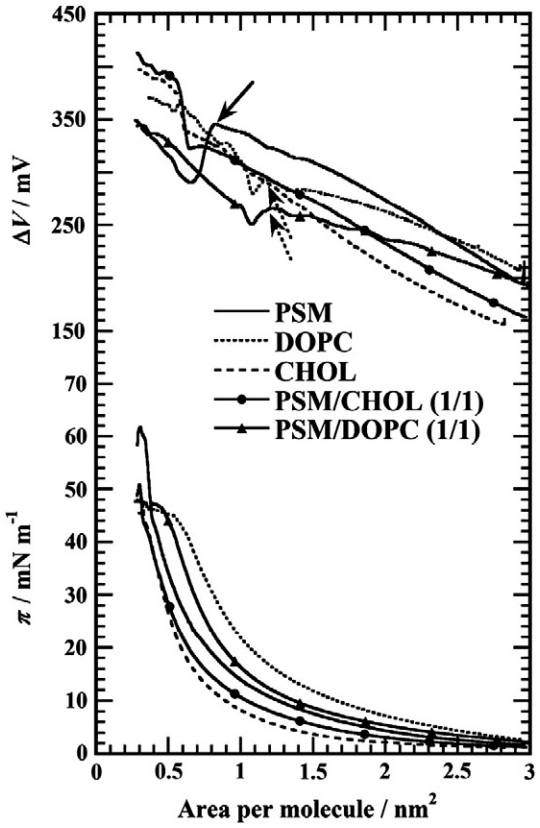

Fig. 10. The π–A and ΔV–A isotherms of one-component (pure PSM, DOPC, and CHOL) and two-component (PSM/CHOL (1/1, mol/mol) and PSM/DOPC (1/1, mol/mol)) monolayers on 0.02 M Tris buffer with 0.13 M NaCl (pH 7.4) at C_{GC} = 50 μM at 298.2 K. Both solid and dashed arrows represent the break point where the slope of ΔV–A isotherms changes negatively. Note that the area axis means mean molecular area of PSM, DOPC, CHOL, and their mixtures, where molecular weight and amount of adsorbed GC are not considered.

the corresponding $\pi - A$ isotherms, GC should be excluded from the surface. Thus, we postulate that GC molecules are desorbed from the surface by compression and then form a surface-associated aggregate just below the CHOL monolayer. This explanation may account for the lack of reduction in ΔV values and is supported by the favorable interaction between CHOL and GC, which can be induced by structural resemblance of the sterol skeleton between them (Fig. 1). Morphological analyses for single and binary monolayers at C_{GC} = 50 μM also reveal the importance of CHOL in the interaction with GC (Fig. S9). Recently, complexation of CHOL and β-GC has been investigated by the nuclear magnetic resonance relaxation [73], which the authors used to show that stoichiometry of stable complexes between β-GC and CHOL is 2:1. This result raises the possibility that two molecules of GC bind to one molecule of CHOL at the air/water interface.

Considering the previously discussed data, isotherm results in Fig. 9 suggest that a large number of GC molecules are gradually desorbed upon compression, and the ternary monolayer is strongly influenced by the adsorbed GC. After its exclusion from the surface, GC remains just below the CHOL monolayer through the attractive interactions between CHOL and GC.

Fig. 11 shows the morphological images of the ternary monolayer as a function of π and C_{GC}. Interestingly, FM and its corresponding BAM images demonstrate that raft domains (dark contrast in FM images) reduce in size, at which LC percentage is maintained constant irrespective of an increase in C_{GC}. That is, the CHOL-rich domain is finely dispersed by surface-associated GC molecules. GC has been reported to lower membrane fluidity, which results in preventing infection from various types of viruses [43]. Our findings denote that GC regulates the size of raft domains from underneath of monolayer to promote the LE network, through which transmitter substances are considered to be transported. Namely, this mechanism may control the fluidity in a cell membrane. To obtain more insight into the expanse of LE networks, the compressibility (Cs^{-1}) values were calculated from $\pi - A$ isotherms (Fig. S10). The results suggest that these values decrease when the amount of GC is increased, which means that the formation of LE network is promoted. However, at a surface pressure of ~35 mN m^{-1}, which corresponds to biomembrane pressure, morphological images show that the distinctive striped GC regions are clearly formed depending on C_{GC} (obviously observed at a concentration of 50 μM), which means that GC divides the ternary monolayer at the interface into pieces. This division by GC is possibly due to a lack of CHOL at the surface relative to the amount of GC, even though two molecules of GC are estimated to bind to one molecule of CHOL [73]. Considering the characteristics of saponins, which exhibit membrane-permeabilizing activity, the striped regions derived from GC may most probably reflect membrane-disrupting activities, the so-called hemolytic activity of saponins [74]. Thus, the GC retained below the surface plays essential roles in the regulation of the raft domain and surrounding fluid networks.

4. Conclusions

In this study, the surface behavior of GC with a lipid raft model consisting of PSM, DOPC, and CHOL was systematically investigated by using the Langmuir monolayer technique. The π–A and ΔV–A isotherms and morphological observations reveal that GC regulates the size of raft

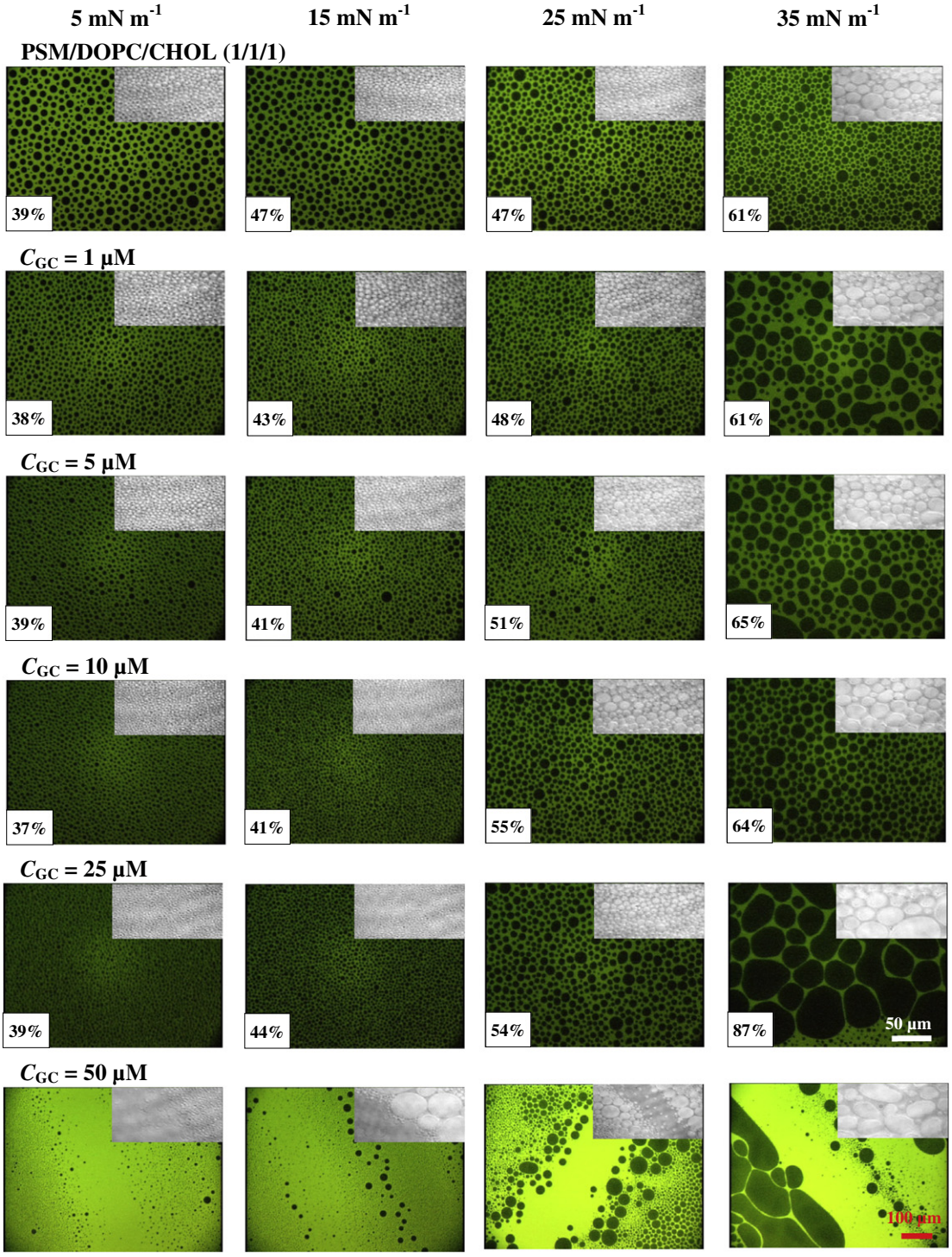

Fig. 11. Fluorescence micrographs of the ternary PSM/DOPC/CHOL (1/1/1, by mol) monolayers at four surface pressures (5, 15, 25, and 35 mN m^{-1}) on 0.02 M Tris buffer with 0.13 M NaCl (pH 7.4) at C_{GC} = 0, 1, 5, 10, 25, and 50 μM at 298.2 K. The monolayers contain 1 mol% of the fluorescent probe (NBD-PC). The white and red scale bars in the lower-right represent 50 μm and 100 μm, respectively. The corresponding BAM images are shown in the upper-right of each photograph. The percentages indicate the ration of occupied LC domains in the frame.

domains from underneath of monolayer to promote the formation of LE network, which plays an important role in the transport of substances via lipid rafts. Because a large amount of GC are found to be squeezed out of the surface upon lateral compression, the retaining GC just below CHOL monolayer plays a key role in the regulation of the size of raft domains and surrounding fluidity networks. In addition, our study using FM and BAM successfully shows activity associated with saponins, i.e., membrane-disrupting activity, at a GC concentration of 50 μM in the subphase despite the degree of GC's hemolytic activity is relatively low. Results of our investigation of the interaction of GC with one- and two-component systems suggest that CHOL is an essential component for formation of distinctive striped regions, which indicate membrane disruption by GC. In general, good and bad effects of saponins represent a double-edged sword. Our findings based on the present monolayer study should allow estimates of effects of saponins' interfacial behavior on biological membranes.

Acknowledgements

The present research was supported by The Japan Food Chemical Research Foundation. This work was also funded by a Grant-in-Aid for Research Activity Start-up [23810030] of the Japan Society for the Promotion of Science (JSPS).

Appendix A. Supplementary data

Supplementary data to this article can be found online at http://dx.doi.org/10.1016/j.bbamem.2013.01.006.

References

[1] I. Fuyuno, Will the sun set on Kampo? Nature 480 (2011) S96.
[2] H. Hayashi, H. Sudo, Economic importance of licorice, Plant Biotechnol. 26 (2009) 101–104.
[3] T.G.J.V. Rossum, A.G. Vulto, R.A.D. Man, J.T. Brouwer, S.W. Schalm, Glycyrrhizin as a potential treatment for chronic hepatitis C, Aliment. Pharmacol. Ther. 12 (1998) 199–205.
[4] H. Akamatsu, J. Komura, Y. Asada, Y. Niwa, Mechanism of anti-inflammatory action of glycyrrhizin: effect on neutrophil functions including reactive oxygen species generation, Planta Med. 57 (1991) 119–121.
[5] S. Amagaya, E. Sugishita, Y. Ogihara, S. Ogawa, K. Okada, T. Aizawa, Comparative studies of the stereoisomers of glycyrrhetinic acid on anti-inflammatory activities, J. Pharmacobiodyn. 7 (1984) 923–928.
[6] D. Steinberg, H.D. Sgan-Cohen, A. Stabholz, S. Pizanty, R. Segal, M.N. Sela, The anticariogenic activity of glycyrrhizin: preliminary clinical trials, Isr. J. Dent. Sci. 2 (1989) 153–157.
[7] S. Thirugnanam, L. Xu, K. Ramaswamy, M. Gnanasekar, Glycyrrhizin induces apoptosis in prostate cancer cell lines DU-145 and LNCaP, Oncol. Rep. 20 (2008) 1387–1392.
[8] J. Cinatl, B. Morgenstern, G. Bauer, P. Chandra, H. Rabenau, H.W. Doerr, Glycyrrhizin, an active component of liquorice roots, and replication of SARS-associated coronavirus, Lancet 361 (2003) 2045–2046.
[9] R. Pompei, O. Flore, M.A. Marccialis, A. Pani, B. Loddo, Glycyrrhizic acid inhibits virus growth and inactivates virus particles, Nature 281 (1979) 689–690.
[10] T. Hattori, S. Ikematsu, A. Koito, S. Matsushita, Y. Maeda, M. Hada, M. Fujimaki, K. Takatsuki, Preliminary evidence for inhibitory effect of glycyrrhizin on HIV replication in patients with AIDS, Antiviral Res. 11 (1989) 255–261.
[11] M. Ito, A. Sato, K. Hirabayashi, F. Tanabe, S. Shigeta, M. Baba, E. De Clercq, H. Nakashima, N. Yamamoto, Mechanism of inhibitory effect of glycyrrhizin on replication of human immunodeficiency virus (HIV), Antiviral Res. 10 (1988) 289–298.
[12] A. Wolkerstorfer, H. Kurz, N. Bachhofner, O.H.J. Szolar, Glycyrrhizin inhibits influenza A virus uptake into the cell, Antiviral Res. 83 (2009) 171–178.
[13] J.-M. Crance, F. Lévêque, E. Biziagos, H. van Cuyck-Gandré, A. Jouan, R. Deloince, Studies on mechanism of action of glycyrrhizin against hepatitis a virus replication in vitro, Antiviral Res. 23 (1994) 63–76.
[14] H. Suzuki, Y. Ohta, T. Takino, K. Fujisawa, C. Hirayama, Effects of glycyrrhizin on biochemical tests in patients with chronic hepatitis-double blind trial, Asian Med. J. 26 (1983) 423–438.
[15] A. Tahara, T. Nakata, Y. Ohtsuka, New type of compound with strong sweetness, Nature 233 (1971) 619–620.
[16] M. Kondo, H. Minamino, G. Okuyama, K. Honda, H. Nagasawa, Y. Otani, Physicochemical properties and applications of α- and β-glycyrrhizins natural surface active agents in licorice root extract, J. Soc. Cosmet. Chem. 37 (1986) 177–189.
[17] A. Otsuka, Y. Yonezawa, K. Iba, T. Tatsumi, H. Sunada, Physico-chemical properties of glycyrrhizic acid in aqueous media. I. Surface-active properties and formation of molecular aggregates, Yakugaku Zasshi 96 (1976) 203–208.
[18] A. Otsuka, Y. Yonezawa, Y. Nakamura, Physico-chemical properties of glycyrrhizic acid in aqueous media. II. Effect on flocculation–deflocculation behavior of suspensions of sulfathiazole and graphite, J. Pharm. Sci. 67 (1978) 151–154.
[19] Y. Yonezawa, A. Otsuka, Physico-chemical properties of glycyrrhizic acid in aqueous media. III. Solubilizing properties for dyes and medicinal substance, YAKUGAKU ZASSHI 101 (1981) 829–835.
[20] E. Azaz, R. Segal, Glycyrrhizin as gelling agents, Pharm. Acta Helv. 55 (1980) 183–186.
[21] K. Simons, E. Ikonen, Functional rafts in cell membranes, Nature 387 (1997) 569–572.
[22] K. Simons, D. Toomre, Lipid rafts and signal transduction, Nat. Rev. Mol. Cell Biol. 1 (2000) 31–39.
[23] D.A. Brown, Seeing is believing: visualization of rafts in model membranes, Proc. Natl. Acad. Sci. 98 (2001) 10517–10518.
[24] J.H. Ipsen, G. Karlstrom, O.G. Mouritsen, H. Wennerstrom, M.J. Zuckermann, Phase equilibria in the phosphatidylcholine-cholesterol system, Biochim. Biophys. Acta 905 (1987) 162–172.
[25] D.J. Recktenwald, H.M. McConnell, Phase equilibria in binary mixtures of phosphatidylcholine and cholesterol, Biochemistry 20 (1981) 4505–4510.
[26] M.B. Sankaram, T.E. Thompson, Interaction of cholesterol with various glycerophospholipids and sphingomyelin, Biochemistry 29 (1990) 10670–10675.
[27] S. Munro, Lipid rafts: elusive or illusive? Cell 115 (2003) 377–388.
[28] A. Radhakrishnan, H.M. McConnell, Cholesterol-phospholipid complexes in membranes, J. Am. Chem. Soc. 121 (1999) 486–487.
[29] J.C. Lawrence, D.E. Saslowsky, J. Michael Edwardson, R.M. Henderson, Real-time analysis of the effects of cholesterol on lipid raft behavior using atomic force microscopy, Biophys. J. 84 (2003) 1827–1832.
[30] N. Periasamy, H. Teichert, K. Weise, R.F. Vogel, R. Winter, Effects of temperature and pressure on the lateral organization of model membranes with functionally reconstituted multidrug transporter LmrA, Biochim. Biophys. Acta 1788 (2009) 390–401.
[31] H.A. Rinia, M.M.E. Snel, J.P.J.M. van der Eerden, B. de Kruijff, Visualizing detergent resistant domains in model membranes with atomic force microscopy, FEBS Lett. 501 (2001) 92–96.
[32] C. Yuan, J. Furlong, P. Burgos, L.J. Johnston, The size of lipid rafts: an atomic force microscopy study of ganglioside GM1 domains in sphingomyelin/DOPC/cholesterol membranes, Biophys. J. 82 (2002) 2526–2535.
[33] K. Hąc-Wydr, P. Dynarowicz-Łątka, P. Wydro, K. Bąk, Edelfosine disturbs the sphingomyelin-cholesterol model membrane system in a cholesterol-dependent way-the Langmuir monolayer study, Colloids Surf. B: Biointerfaces 88 (2011) 635–640.
[34] E. Prenner, G. Honsek, D. Hönig, D. Möbius, K. Lohner, Imaging of the domain organization in sphingomyelin and phosphatidylcholine monolayers, Chem. Phys. Lipids 145 (2007) 106–118.
[35] K. Bacia, D. Scherfeld, N. Kahya, P. Schwille, Fluorescence correlation spectroscopy relates rafts in model and native membranes, Biophys. J. 87 (2004) 1034–1043.
[36] T. Baumgart, S.T. Hess, W.W. Webb, Imaging coexisting fluid domains in biomembrane models coupling curvature and line tension, Nature 425 (2003) 821–824.
[37] R.F.M. de Almeida, J. Borst, A. Fedorov, M. Prieto, A.J.W.G. Visser, Complexity of lipid domains and rafts in giant unilamellar vesicles revealed by combining imaging and microscopic and macroscopic time-resolved fluorescence, Biophys. J. 93 (2007) 539–553.
[38] J. Juhasz, F.J. Sharom, J.H. Davis, Quantitative characterization of coexisting phases in DOPC/DPPC/cholesterol mixtures: comparing confocal fluorescence microscopy and deuterium nuclear magnetic resonance, Biochim. Biophys. Acta 1788 (2009) 2541–2552.
[39] M.T. Stöckl, A. Herrmann, Detection of lipid domains in model and cell membranes by fluorescence lifetime imaging microscopy, Biochim. Biophys. Acta 1798 (2010) 1444–1456.
[40] S.L. Veatch, I.V. Polozov, K. Gawrisch, S.L. Keller, Liquid domains in vesicles investigated by NMR and fluorescence microscopy, Biophys. J. 86 (2004) 2910–2922.
[41] G. Wheeler, K.M. Tyler, Widefield microscopy for live imaging of lipid domains and membrane dynamics, Biochim. Biophys. Acta 1808 (2011) 634–641.
[42] T. Nakamura, T. Fujii, A. Ichihara, Enzyme leakage due to change of membrane permeability of primary cultured rat hepatocytes treated with various hepatotoxins and its prevention by glycyrrhizin, Cell. Biol. Toxicol. 1 (1985) 285–295.
[43] S. Harada, The broad anti-viral agent glycyrrhizin directly modulates the fluidity of plasma membrane and HIV-1 envelope, Biochem. J. 392 (2005) 191–199.
[44] A.D. Bangham, R.W. Horne, A.M. Glauert, J.T. Dingle, J.A. Lucy, Action of saponin on biological cell membranes, Nature 196 (1962) 952–955.
[45] E. Baumann, G. Stoya, A. Völkner, W. Richter, C. Lemke, W. Linss, Hemolysis of human erythrocytes with saponin affects the membrane structure, Acta Histochem. 102 (2000) 21–35.
[46] M. Chwalek, N. Lalun, H. Bobichon, K. Plé, L. Voutquenne-Nazabadioko, Structure-activity relationships of some hederagenin diglycosides: haemolysis, cytotoxicity and apoptosis induction, Biochim. Biophys. Acta 1760 (2006) 1418–1427.
[47] R.R. Dourmashkin, R.M. Dougherty, R.J. Harris, Electron microscopic observations on Rous sarcoma virus and cell membranes, Nature 194 (1962) 1116–1119.
[48] P. Seeman, D. Cheng, G.H. Iles, Structure of membrane holes in osmotic and saponin hemolysis, J. Cell. Biol. 56 (1973) 519–527.
[49] C.N. Armah, A.R. Mackie, C. Roy, K. Price, A.E. Osbourn, P. Bowyer, S. Ladha, The membrane-permeabilizing effect of avenacin A-1 involves the reorganization of bilayer cholesterol, Biophys. J. 76 (1999) 281–290.
[50] E.A.J. Keukens, T. de Vrije, C. van den Boom, P. de Waard, H.H. Plasman, F. Thiel, V. Chupin, W.M.F. Jongen, B. de Kruijff, Molecular basis of glycoalkaloid induced membrane disruption, Biochim. Biophys. Acta 1240 (1995) 216–228.
[51] F. Lin, R. Wang, Hemolytic mechanism of dioscin proposed by molecular dynamics simulations, J. Mol. Model. 16 (2010) 107–118.
[52] H. Nakahara, O. Shibata, Y. Moroi, Examination of surface adsorption of cetyltrimethylammonium bromide and sodium dodecyl sulfate, J. Phys. Chem. B 115 (2011) 9077–9086.
[53] C.L. Wennberg, D. van der Spoel, J.S. Hub, Large influence of cholesterol on solute partitioning into lipid membranes, J. Am. Chem. Soc. 134 (2012) 5351–5361.
[54] (a) R. Maget-Dana, The monolayer technique: a potent tool for studying the interfacial properties of antimicrobial and membrane-lytic peptides and their interactions with lipid membranes, Biochim. Biophys. Acta 1462 (1999) 109–140;
(b) V. Vogel, D. Möbius, Local surface potentials and electric dipole moments of lipid monolayers: contributions of the water/lipid and the lipid/air interfaces, J. Colloid Interface Sci. 126 (1988) 408–420.
[55] M.L. Fanani, B. Maggio, Liquid–liquid domain miscibility driven by composition and domain thickness mismatch in ternary lipid monolayers, L. Phys. Chem. B 115 (2011) 41–49.
[56] H. Brockman, Dipole potential of lipid membranes, Chem. Phys. Lipids 37 (1994) 57–79.
[57] S.A. Simon, T.J. McIntosh, Magnitude of the solvation pressure depends on dipole potential, Proc. Natl. Acad. Sci. U. S. A. 86 (1989) 9263–9267.
[58] H. Nakahara, S. Lee, M.P. Krafft, O. Shibata, Fluorocarbon-hybrid pulmonary surfactants for replacement therapy — a Langmuir monolayer study, Langmuir 26 (2010) 18256–18265.

[59] G.L. Gaines Jr., Insoluble Monolayers at Liquid–Gas Interfaces, Interscience, New York, 1966, p. 288.
[60] J. Marsden, J.H. Schulman, Molecular interaction in monolayers, Trans. Faraday Soc. 34 (1938) 748–758.
[61] D.O. Shah, J.H. Schulman, Influence of calcium, cholesterol, and unsaturation on lecithin monolayers, J. Lipid Res. 8 (1967) 215–226.
[62] (a) P. Dynarowicz-Łatka, K. Hąc-Wydro, Interactions between phosphatidylcholines and cholesterol in monolayers at the air/water interface, Colloids Surf. B: Biointerfaces 37 (2004) 21–25;
(b) P. Wydro, S. Knapczyk, M. Lapczyńska, Variations in the condensing effect of cholesterol on saturated versus unsaturated phosphatidylcholines at low and high sterol concentration, Langmuir 27 (2011) 5433–5444.
[63] Y. Barenholz, T.E. Thompson, Sphingomyelins in bilayers and biological membranes, Biochim. Biophys. Acta 604 (1980) 129–158.
[64] A. Björkbom, T. Róg, P. Kankaanpää, D. Lindroos, K. Kaszuba, M. Kurita, S. Yamaguchi, T. Yamamoto, S. Jaikishan, L. Paavolainen, J. Päivärinne, T.K.M. Nyholm, S. Katsumura, I. Vattulainen, J.P. Slotte, N- and O-methylation of sphingomyelin markedly affects its membrane properties and interactions with cholesterol, Biochim. Biophys. Acta 1808 (2011) 1179–1186.
[65] H. Yokoyama, H. Nakahara, T. Nakagawa, S. Shimono, K. Sueishi, O. Shibata, Miscibility behavior of two-component monolayers at the air–water interface: perfluorocarboxylic acids and DMPE, J. Colloid Interface Sci. 337 (2009) 191–200.
[66] H. Nakahara, M.P. Krafft, A. Shibata, O. Shibata, Interaction of a partially fluorinated alcohol (F8H11OH) with biomembrane constituents in two-component monolayers, Soft Matter 7 (2011) 7325–7333.
[67] P. Joos, R.A. Demel, The interaction energies of cholesterol and lecithin in spread mixed monolayers at the air–water interface, Biochim. Biophys. Acta 183 (1969) 447–457.
[68] L.J. Pike, X. Han, K.-N. Chung, R.W. Gross, Lipid rafts are enriched in arachidonic acid and plasmenylethanolamine and their composition is independent of caveolin-1 expression: a quantitative electrospray ionization/mass spectrometric analysis, Biochemistry 41 (2002) 2075–2088.
[69] R.A. Demel, W.S.M. Geurts Van Kessel, R.F.A. Zwaal, B. Roelofsen, L.L.M. Van Deenen, Biochim. Biophys. Acta 406 (1975) 97–107.
[70] R.A. Demel, Monomolecular layers in the study of biomembranes, Subcell. Biochem. 23 (1994) 83–120.
[71] D. Marsh, Lateral pressure in membranes, Biochim. Biophys. Acta 1286 (1996) 183–223.
[72] R.F.M. de Almeida, A. Fedorov, M. Prieto, Sphingomyelin/phosphatidylcholine/cholesterol phase diagram: boundaries and composition of lipid rafts, Biophys. J. 85 (2003) 2406–2416.
[73] O.Y. Gluschenko, N.E. Polyakov, T.V. Leshina, NMR relaxation study of cholesterol binding with plant metabolites, Appl. Magn. Reson. 41 (2011) 283–294.
[74] J.M. Augustin, V. Kuzina, S.B. Andersen, S. Bak, Molecular activities, biosynthesis and evolution of triterpenoid saponins, Phytochemistry 72 (2011) 435–457.